Tide-driven shear instability in planetary liquid cores

Alban Sauret[1,2], Michael Le Bars[1], and Patrice Le Gal[1]

[1] Aix Marseille Université, CNRS, Centrale Marseille, IRPHE UMR 7342, Marseille, France, [2] Department of Mechanical and Aerospace Engineering, Princeton University, Princeton, New Jersey, USA

Abstract We present an experimental study on the shear instability driven by tidal forcing in a model planetary liquid core. The experimental setup consists of a water-filled deformable sphere rotating around its axis and subjected to an elliptical forcing. At resonant forcing frequencies, the nonlinear self-interaction of the excited inertial mode drives an intense and localized axisymmetric jet. The jet becomes unstable at low Ekman number because of a shear instability. Using particle image velocimetry measurements, we derive a semiempirical scaling law that captures the instability threshold of the shear instability. This mechanism is fully relevant to planetary systems, where it constitutes a new route to generate turbulence in their liquid cores.

1. Introduction

Rotation of planets is always perturbed by gravitational interactions with their companions that generate perturbations of their shape, of the direction of their rotational vector, and of their rotation rate [see, e.g., *Olson*, 2013]. Those perturbations correspond to tidal distortions [*Malkus*, 1989; *Cébron et al.*, 2012, 2013], precession/nutation motions [*Malkus*, 1968; *Noir et al.*, 2001], and librations [*Noir et al.*, 2009; *Busse*, 2010; *Sauret and Le Dizès*, 2013], respectively. The mechanical forcings are generally of small amplitude. Yet they can be of critical importance in planetary cores as they can drive inertial modes, zonal flows, and instabilities, generating turbulence [e.g., *Aldridge and Lumb*, 1987; *Kuhn et al.*, 2000; *Morize et al.*, 2010; *Sauret et al.*, 2010; *Zhang et al.*, 2011; *Sauret et al.*, 2012; *Cébron et al.*, 2012b; *Noir et al.*, 2012; *Sauret et al.*, 2013]. Flows driven by mechanical forcings can thus provide alternative mechanisms to the standard convective models [see, e.g., *Glatzmaier and Roberts*, 1995; *Aurnou and Olson*, 2001] in rationalizing the variety of magnetic fields observed in planets of our solar system and in extrasolar ones. For instance, mechanical forcings provide plausible scenarios to explain the Moon's past magnetic field [*Le Bars et al.*, 2011; *Dwyer et al.*, 2011]. In this letter, we show that the localized nonlinear flow excited by a tidal forcing at a resonant frequency can become unstable following a shear instability that generates turbulence. We study experimentally the consequences of an elliptical deformation on a rotating sphere filled with water. This experimental system is a model of a tidally deformed liquid core. We note that other harmonic forcings such as precession and libration are expected to excite the same generic mechanism [see, e.g., *Vanyo et al.*, 1995].

2. Inertial Modes and Zonal Flow

So-called inertial modes associated with the Coriolis force develop in any enclosed rotating fluid. These modes are usually damped by viscosity, but they can be excited by harmonic forcings whose frequencies range between plus and minus twice the spin frequency [*Greenspan*, 1968]. Recent numerical simulations [*Tilgner*, 2007] and laboratory experiments [*Morize et al.*, 2010] have considered the inertial modes excited by tidal deformations in a spherical container. They show that the ratio of the rotation rate of the tides (i.e., the orbital rotation rate of the companion) to the rotation rate of the considered planet determines the inertial modes excited in the system. The base flow driven by tidal distortion has an azimuthal wave number $m = 2$. This base flow generates a flow of azimuthal wave number $m = 4$ and an axisymmetric contribution $m = 0$, the so-called zonal flow, through nonlinear self-interaction. Experimentally, *Morize et al.* [2010] have shown that the axisymmetric flow generated in the bulk is small except when the frequency of the forcing matches an eigenmode of the sphere. In this situation, a localized intense geostrophic zonal jet appears in the bulk. Their experiments exhibit a clear dependence of the associated maximal azimuthal velocity on the square of the tidal amplitude. The purpose of this paper is to further investigate this dynamics when decreasing the Ekman number, i.e., the ratio of the viscous to the Coriolis forces, which is very small in planetary cores.
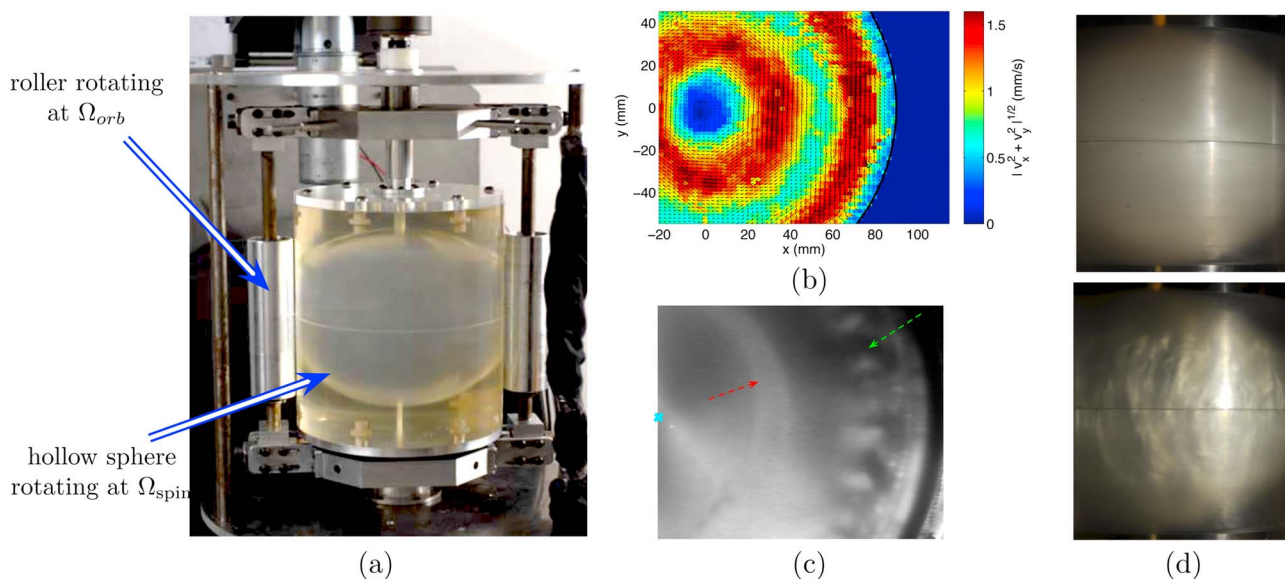
Figure 1. (a) Picture of the experimental setup. (b) Horizontal velocity field in the equatorial plane measured in the rotating frame for $\varepsilon = 0.045$, $E = 1.25 \times 10^{-5}$, and $\Omega_R = 0.384$. The center of the sphere is at (0, 0). (c) Top view of the flow structure in the equatorial plane with Kalliroscope flakes corresponding to the unstable case in Figure 1d. The blue cross is the center of the sphere. The red arrow points to a stable shear region whereas the green arrow points to an unstable shear region. (d) Bulk visualization from the side of stable (top: $\varepsilon = 0.045$) and unstable (bottom: $\varepsilon = 0.075$) flows, respectively, for $E = 1.25 \times 10^{-5}$ and $\Omega_R = 0.384$.

3. Experimental Setup

The experimental setup (Figure 1a) consists of a hollow sphere of radius $R = 10$ cm and cast in a silicone gel that is both deformable and transparent to allow direct flow visualization [see also *Le Bars et al.*, 2010; *Sauret et al.*, 2010; *Morize et al.*, 2010]. The sphere is filled with water (kinematic viscosity $\nu = 10^{-6} \mathrm{m^2/s}$) and set in rotation about its vertical axis (Oz) at a constant angular velocity in the range $\Omega_{\mathrm{spin}} \in [2; 19]$ rad·s^{-1} with a accuracy of $\pm 0.3\%$. In addition, to generate a tidal deformation on the rotating sphere, two vertical cylindrical rollers are applied symmetrically on the sphere and rotate independently at a constant angular velocity $\Omega_{\mathrm{orb}} \in [2; 12]$ rad·s^{-1} with a accuracy of $\pm 0.3\%$. Our system is fully described by three dimensionless parameters. The Ekman number $E = \nu/(\Omega_{\mathrm{spin}} R^2)$ is the ratio of viscous to Coriolis effects. In the present study, E varies between 5×10^{-6} and 8×10^{-5}. We also define the ratio of the orbital to the spin angular rotation rate, $\Omega_R = \Omega_{\mathrm{orb}}/\Omega_{\mathrm{spin}}$, referred to as the forcing frequency, and the amplitude of the tidal deformation $\varepsilon = 0.02 - 0.09 \pm 3 \times 10^{-3}$, that is equal to twice the tidal bulge divided by R.

To obtain a quantitative insight into the flow generated by the tidal forcing, we perform measurements using a particle image velocimetry (PIV) system corotating with the sphere (see *Morize et al.* [2010] for details). *Morize et al.* [2010] calculated the mean zonal flow by taking one picture per rotation. Continuous recording of the flow at 24 frames per second, PIV processing the successive frames, and averaging the obtained velocity field over more than 70 rotations allow us to increase the accuracy of the measurement. To conduct this measurement, we use a miniature wireless camera (Video Camera of dimensions 2 cm × 2 cm, and of resolution 576×768 pixels, 24 frames per second) that rotates at constant angular velocity Ω_{spin} and measures the flow in the equatorial plane from above through the transparent top surface. The PIV particles of diameter 100 μm are illuminated by a laser sheet of thickness 3 mm, produced by a continuous laser (8 W). We start the measurements after the transient spin-up, typically 10 min after the onset of the rotation. Figure 1b shows a typical velocity field measured in the equatorial plane at a resonant forcing. The presence and stability of shear layers is also observed through qualitative visualizations using anisotropic particles (Kalliroscope flakes) illuminated in the equatorial plane (see Figure 1c) or from the side (Figure 1d). This qualitative approach permits to determine the threshold of the instability.

4. Shear Instability

The influence of the forcing frequency on the amplitude of the mean zonal flow has been characterized by *Morize et al.* [2010]. They have shown that the amplitude of the mean zonal flow remains small except
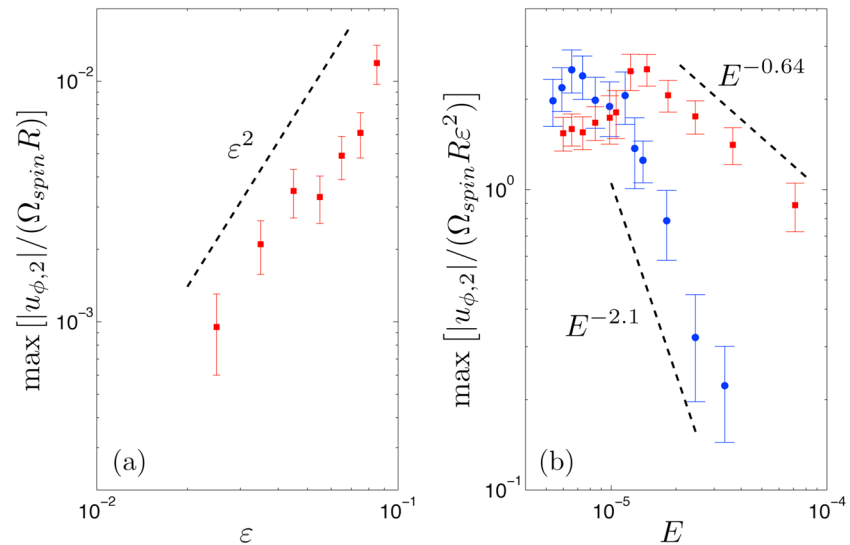
Figure 2. (a) Maximal azimuthal velocity associated to the mean zonal flow rescaled by $\Omega_{\text{spin}} R$ for $E = 9.46 \times 10^{-6}$ and $\Omega_R = 0.384$. The dashed line shows the scaling ε^2. (b) Maximal azimuthal velocity associated to the mean zonal flow rescaled by $\Omega_{\text{spin}} R\varepsilon^2$ for $\varepsilon = 0.045$ and $\Omega_R = 0.384$ (red squares) and $\Omega_R = 0.178$ (blue circles). The dashed lines show the best fits of slope $E^{-0.64\pm0.08}$ and $E^{-2.1\pm0.4}$, respectively. Note that in the previous study by *Morize et al.* [2010], the scaling $E^{-3/10}$ was mentioned for the resonance at $\Omega_R = 0.38$: the resonance band of a given inertial mode in Ω_R being very thin around its resonance frequency, a small change in the excitation frequency apparently leads to rapid changes in the scaling behavior of the zonal jet.

when the orbital frequency resonates with an eigenmode of the sphere. In the following we mainly consider the resonance at the forcing frequency $\Omega_R = 0.384$, which is the easiest excitable mode in our system (Figure 1b) and allows the most accurate measurements of the corresponding velocity field. We note that other eigenmodes of the sphere can also be excited at Ekman numbers accessible to our experimental setup, for instance at $\Omega_R = 0.178$. Figure 2 shows the influence of the dimensionless parameters on the internal zonal jet. We plot the evolution of the maximum amplitude of the zonal flow as a function of the amplitude of the tidal deformation ε in Figure 2a. As expected the amplitude of the mean zonal flow scales as the square of the deformation (ε^2), which is consistent with the results previously obtained by *Morize et al.* [2010]. However, we observe a localized change in the general trend of the curve between $\varepsilon = 0.045$ and $\varepsilon = 0.055$ for an Ekman number $E = 9.46 \times 10^{-6}$. We shall see in the following that at this Ekman number and for this particular mode, $\varepsilon \simeq 0.045$ corresponds to the threshold for destabilization of the jet by a shear instability that modifies the structure of the flow.

We then study the dependence of the maximum azimuthal velocity associated with the mean zonal flow as a function of the Ekman number E for a fixed tidal deformation $\varepsilon = 0.045$ and for a forcing frequency $\Omega_R = 0.384$ (see Figure 2b). We note that the velocity of the zonal flow for this mode is proportional to $E^{-0.64\pm0.08}$ and emphasize that this exponent cannot be generalized to the other forced modes, at least for the Ekman numbers considered in our experiments ($E > 5 \times 10^{-6}$). For example, Figure 2b also shows the velocity of the zonal flow for $\Omega_R = 0.178$, which is then proportional to $E^{-2.1\pm0.4}$. We expect this change of exponent to be due to finite Ekman number effects since the asymptotic regime for inertial modes is only reached for $E < 10^{-8}$ [*Rieutord and Valdettaro*, 2010]. This feature was also observed numerically in a spherical shell for a tidal forcing [*Favier et al.*, 2014]. However, Figure 2b shows that for both resonant forcing frequencies, the measured zonal flow saturates at low Ekman number. This saturation coincides with the destabilization of the geostrophic flow observed in experiments with Kalliroscope particles (see Figure 1d). We expect this mechanism of flow destabilization at low Ekman number to be generic to any resonant forcing frequency.

A top view of the flow patterns in the equatorial plane is shown in Figure 1c and illustrates the presence of a nonaxisymmetric instability reminiscent of the one observed in differentially rotating spherical shell by *Schaeffer and Cardin* [2005]. We have systematically explored the transition between stable and unstable regimes using such type of experiments. We define the critical deformation ε_c as the minimum value of ε for which the flow is unstable at a given Ekman number. The experimental results are reported in Figure 3 for
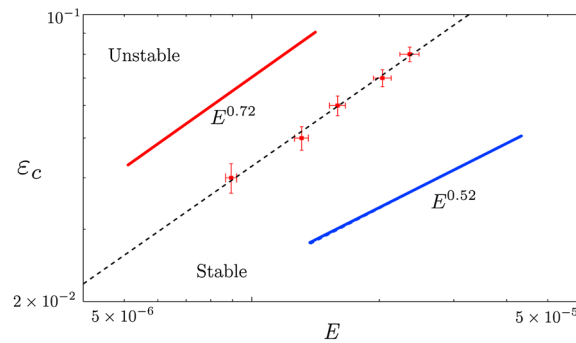
Figure 3. Stability threshold of the inner band for the mode excited at $\Omega_R = 0.384$. The red squares are the experimental results with the error bars. The black dashed line shows the best fit of the experimental points $\varepsilon_c \sim E^{0.68}$. The red line shows the slope of the semiempirical scaling law based on a viscous damping, $\varepsilon_c \sim E^{0.72}$, and the blue line the slope of the semiempirical scaling law based on a beta effect, $\varepsilon_c \sim E^{0.52}$.

the zonal jet located around $r \sim 0.4$ at the forcing frequency $\Omega_R = 0.384$. The best fit of the experimental measurements gives the following threshold:

$$\varepsilon_c \propto E^{0.68 \pm 0.11}, \tag{1}$$

where the limited range of explored Ekman numbers implies a rather large uncertainty on the experimentally determined exponent. This scaling law can be rationalized using a simplified model presented in the next paragraph.

5. Semiempirical Scaling Law

The structure of the flow shown in Figure 1c is typical of the patterns induced by a shear instability in a rotating flow [*Kuo*, 1949; *Busse*, 1968; *Fruh and Read*, 1999; *Hollerbach*, 2003; *Schaeffer and Cardin*, 2005; *Guervilly et al.*, 2012]. This instability is generated by rapid changes of the local rotation rate over a short distance. Previous authors estimated that an instability occurs when the local Rossby number, $R_o = \Delta\Omega/\Omega_{spin}$ reaches a critical value $R_{o,c}$, where $\Delta\Omega$ stands for the change in the rotation rate in the jet. To determine the instability threshold, we consider the two extreme cases introduced by *Schaeffer and Cardin* [2005] for the "split sphere" and the "differential inner core rotation" configurations. In all three configurations, the source of the instability is the shear, measured by $R_o/(\Delta r)^2$, where Δr is the thickness of the shear layer. The threshold is determined by balancing this source term with the damping term. In a spherical geometry, the damping is dominated either by the viscous dissipation scaling as $E\,m^3$, where m is the critical wave number taken as $m \sim (\Delta r)^{-1}$, or by the β effect related to the change of depth of the fluid column as a function of the distance r from the axis, scaling as $\beta = r/(1 - r^2)$. We now need to estimate R_o and Δr as function of E and ε in our flow. The shear layers considered in our configuration are generated by the nonlinear effects in the Ekman layer of the oscillatory flow driven by the harmonic tidal forcing. The corresponding natural lengthscale in the sphere is $\Delta r \sim E^{1/5}$, as shown by *Kerswell* [1995] and validated in the closely related case of harmonic *precession* forcing by *Kida* [2011]. Note in particular that this scaling is different from the one relevant for a Stewartson layer [*Stewartson*, 1966], which applies to the split sphere and to the differential inner core rotation configurations [*Schaeffer and Cardin*, 2005]. Note also that in the spherical shell, the relevant lengthscale for a shear layer driven by an harmonic mechanical forcing is $\Delta r \sim E^{1/3}$ [*Kerswell*, 1995; *Tilgner*, 2007]. Regarding the Rossby number, to the best of our knowledge, no analytical description of the amplitude of zonal jets induced by a resonant forcing of inertial modes has been determined. We thus use the amplitude measured experimentally as shown in Figure 2b, and obtain $R_o \sim \varepsilon^2 E^{-0.64 \pm 0.08}$, where $\Delta\Omega = |\Delta u_{\phi,2}|/r$. Depending on the main source of damping, two scaling laws for the shear instability threshold can then be derived: considering the viscous damping leads to $\varepsilon_c \sim E^{0.72 \pm 0.04}$, while considering the β effect leads to $\varepsilon_c \sim E^{0.52 \pm 0.04}$. These two scalings are compared with the experimental measurements in Figure 3. For this type of flow, in the range of parameters explored by our setup and for the considered shear layer, the comparison between the semiempirical scaling law and the best fitting experimental law suggests that the viscous effects dominate over the curvature effect. This does not preclude that the β effect may become predominant for shear layers located at larger r and/or at smaller Ekman number, but this will have to be explored using another setup or another method.

6. Discussions and Conclusions

At resonant frequencies, tidal forcings generate zonal flows that become unstable at small Ekman number leading to turbulence. In the present experimental study, we characterize the destabilization of the mean zonal flow for the most easily excited mode in our setup ($\Omega_R = 0.384$). We also observe the presence of the same shear instability for other experimentally excitable resonances, for instance at $\Omega_R = 0.178$ for which the critical deformation would scale as $\varepsilon_c \sim E^{1.45 \pm 0.2}$ considering the viscous damping (see previous paragraph for detailed derivation). Future research will have to consider the presence of an inner core, as

Table 1. Physical Characteristics Used for the Planetary Calculations Presented in Figure 4[a]

|	Earth	Primitive Earth	Mars	Venus	Mercury
M ($\times 10^{-24}$ kg)	5.98	5.98	0.642	4.87	0.33
R (km)	6378	6378	3390	6051	2440
T_{spin} (days)	0.997	0.418	1.026	−243	58.6
R_{core}/R	0.55	0.55	0.44	0.17	0.8
E ($\times 10^{14}$)	0.11	0.047	0.61	316	21
ε ($\times 10^{7}$)	1.4	8.9	0.16	1.1	7.1

[a]Tidal amplitudes are computed using the hydrostatic hypothesis.

the scaling of the zonal flow could then be different. But we expect that the presence of an inner core does not modify the generic mechanism of the shear instability shown here nor its physical description; it should only change the scaling law for the threshold. For instance, *Tilgner* [2007] shows numerically that in the shell, the zonal flow varies as $u_{\phi,2} \sim \varepsilon^2 E^{-3/4}$, and the thickness of the shear layer over which the shear instability appears is now proportional to $\Delta r \sim E^{1/3}$ [see also *Ogilvie*, 2005; *Rieutord and Valdettaro*, 2010]. Using the analytical description detailed in section 5, we obtain for the shell a scaling law of the critical deformation, $\varepsilon_c \sim E^{17/24}$, which is valid for the two types of damping processes described above, i.e., viscous damping and β effect. Note that this exponent corresponds to a greater tendency toward flow destabilization when compared to our experimental law equation (1).

In planets, the Ekman number is so small that any tidal forcing in the range of inertial frequencies may excite a resonant mode. As a first step toward geophysical applications, let us extrapolate the experimental scaling law (1), including its uncertainty on the scaling exponent, to planetary values of the Ekman number and the tidal deformation. Note again that its exponent is determined experimentally for moderate values of the Ekman number. But its exponent is the smallest one compared to the other cases discussed above, leading to the most conservative estimate of the threshold. Relevant parameters are given in Table 1 and results are reported in Figure 4. The generic mechanism shown here is susceptible to happen in telluric bodies of the Solar System, where it would constitute an alternative route toward core turbulence. Based on the experimental results presented above and acknowledging their limitations, the present Earth, Mercury, and Mars are potentially unstable to the shear instability, and the early Earth and early Mars with its ancient moon are unstable.

In conclusion, we have shown experimentally a new generic route toward turbulence in a rotating spherical fluid layer subject to a harmonic mechanical forcing. Additional studies are now necessary to fully evaluate the relevance of this process in planets. Among the open questions, we would like to stress the following three. First, systematic experiments and/or calculations at smaller Ekman number and in presence of an inner core are now needed to provide a complete description of the generated turbulence and in particular to determine the spatial extension of the turbulent zone and the typical power spectrum. Then, it would also be interesting to evaluate the interaction of the process shown here with the other ingredients potentially present in planetary cores, such as a convective flow or a magnetic field. Finally, the possibility to generate a dynamo using such a shear layer instability mechanism remains a stimulating challenge [see, e.g., *McWilliams*, 2012; *Zimmerman et al.*, 2014].
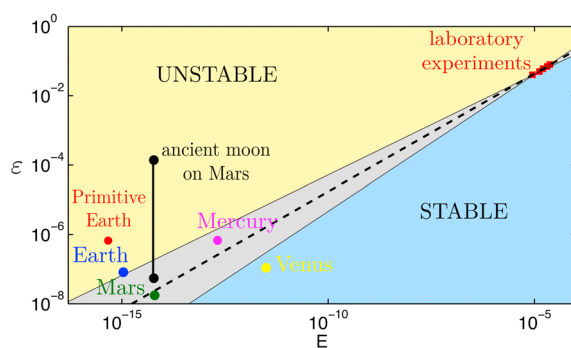
Figure 4. Stability of the zonal jet generated in liquid cores of planets evaluated using the parameters of Table 1. The red squares are the experimental results, the black dashed line of slope $E^{0.68}$ represents the best fit determined experimentally, and the grey zone takes into account the uncertainty on the scaling exponent. The thick black line is extracted from *Arkani-Hamed* [2009] and corresponds to the tides generated by an ancient moon on Mars.

References

Aldridge, K. D., and L. I. Lumb (1987), Inertial waves identified in the Earth's fluid outer core, *Nature*, *421–423*, 325.

Arkani-Hamed, J. (2009), Did tidal deformation power the core dynamo of Mars?, *Icarus*, *201*(1), 31–43.

Aurnou, J. M., and P. L. Olson (2001), Strong zonal winds from thermal convection in a rotating spherical shell, *Geophys. Res. Lett.*, *28*, 2557–2559, doi:10.1029/2000GL012474.

Busse, F. H. (1968), Shear flow instabilities in rotating systems, *J. Fluid Mech.*, *33*, 577–589.

Busse, F. H. (2010), Mean zonal flows generated by librations of a rotating spherical cavity, *J. Fluid Mech.*, *650*, 505–512.

Cébron, D., M. Le Bars, C. Moutou, and P. Le Gal (2012), Elliptical instability in terrestrial planets and moons, *Astron. Astrophys.*, *539*, 1–16.

Cébron, D., M. Le Bars, J. Noir, and J. M. Aurnou (2012b), Libration driven elliptical instability, *Phys. Fluids*, *24*(061,703), doi:10.1063/1.4729296.

Cébron, D., M. Le Bars, P. Le Gal, C. Moutou, J. Leconte, and A. Sauret (2013), Elliptical instability in hot-Jupiter systems, *Icarus*, *226*(2), 1642–1653.

Dwyer, C. A., D. J. Stevenson, and F. Nimmo (2011), A long-lived lunar dynamo driven by continuous mechanical stirring, *Nature*, *479*, 212–214.

Favier, B., A. J. Barker, and C. Baruteau (2014), Non-linear evolution of tidally forced inertial waves in rotating fluid bodies, *Mon. Not. R. Astron. Soc.*, *439*(1), 845–860.

Fruh, W. G., and P. L. Read (1999), Experiments on a barotropic rotating shear layer. Part 1. Instability and steady vortices, *J. Fluid Mech.*, *383*(1), 143–173.

Glatzmaier, G. A., and P. H. Roberts (1995), A three-dimensional self-consistent computer simulation of a geomagnetic field reversal, *Nature*, *377*, 203–209.

Greenspan, H. P. (1968), *The Theory of Rotating Fluids*, Cambridge Univ. Press, Cambridge, U. K.

Guervilly, C., P. Cardin, and N. Schaeffer (2012), A dynamo driven by zonal jets at the upper surface: Applications to giant planets, *Icarus*, *218*, 100–114.

Hollerbach, R. (2003), Instabilities of the Stewartson layer. Part 1. The dependence on the sign of Ro, *J. Fluid Mech.*, *492*, 289–302.

Kerswell, R. R. (1995), On the internal shear layers spawned by the critical regions in oscillatory Ekman boundary layers, *J. Fluid Mech.*, *298*, 311–325.

Kida, S. (2011), Steady flow in a rapidly rotating sphere with weak precession, *J. Fluid Mech.*, *680*, 150–193.

Kuhn, J. R., J. D. Amstrong, R. I. Bush, and P. Scherrer (2000), Rossby waves on the Sun as revealed by solar hills, *Nature*, *405*, 544–546.

Kuo, H.-L. (1949), Dynamic instability of two-dimensional non divergent flow in a barotropic atmosphere, *J. Meteorol.*, *6*, 105–122.

Le Bars, M., L. Lacaze, S. Le Dizès, P. Le Gal, and M. Rieutord (2010), Tidal instability in stellar and planetary binary systems, *Phys. Earth Planet. Inter.*, *178*, 48-55.

Le Bars, M., M. A. Wieczorek, O. Karatekin, D. Cébron, and M. Laneuville (2011), An impact-driven dynamo for the early moon, *Nature*, *479*, 215–218.

Malkus, W. V. R. (1968), Precession of the Earth as the cause of geomagnetism, *Science*, *160*, 259–264.

Malkus, W. V. R. (1989), An experimental study of global instabilities due to tidal (elliptical) distorsion of a rotating elastic cylinder, *Geophys. Astrophys. Fluid Dynam.*, *48*, 123–134.

McWilliams, J. C. (2012), The elemental shear dynamo, *J. Fluid Mech.*, *699*, 414–452.

Morize, C., M. Le Bars, P. Le Gal, and A. Tilgner (2010), Experimental determination of zonal winds driven by tides, *Phys. Rev. Lett.*, *99*, 214501, doi:10.1103/PhysRevLett.104.214501.

Noir, J., D. Brito, K. Aldridge, and P. Cardin (2001), Experimental evidence of inertial waves in a precessing spheroidal cavity, *Geophys. Res. Lett.*, *28*(19), 3785–3788, doi:10.1029/2001GL012956.

Noir, J., F. Hemmerlin, J. Wicht, S. M. Baca, and J. M. Aurnou (2009), An experimental and numerical study of librationally driven flow in planetary cores and subsurface oceans, *Phys. Earth Planet. Int.*, *173*, 141–152.

Noir, J., D. Cébron, M. Le Bars, A. Sauret, and J. M. Aurnou (2012), Experimental study of libration-driven zonal flows in non-axisymmetric containers, *Phys. Earth Planet. Int.*, *204*, 1–10.

Ogilvie, G. I. (2005), Wave attractors and the asymptotic dissipation rate of tidal disturbances, *J. Fluid Mech.*, *543*, 19–44.

Olson, P. (2013), Experimental dynamos and the dynamics of planetary cores, *Annu. Rev. Earth Planet. Sci.*, *41*, 153–181.

Rieutord, M., and L. Valdettaro (2010), Viscous dissipation by tidally forced inertial modes in a rotating spherical shell, *J. Fluid Mech.*, *643*, 363–394.

Sauret, A., and S. Le Dizès (2013), Libration-induced mean flow in a spherical shell, *J. Fluid Mech.*, *718*, 181–209.

Sauret, A., D. Cébron, C. Morize, and M. Le Bars (2010), Experimental and numerical study of mean zonal flows generated by librations of a rotating spherical cavity, *J. Fluid Mech.*, *662*, 260–268.

Sauret, A., D. Cébron, M. Le Bars, and S. Le Dizès (2012), Fluid flows in a librating cylinder, *Phys. Fluids*, *24*, 026603, doi:10.1063/1.3680874.

Sauret, A., D. Cébron, and M. Le Bars (2013), Spontaneous generation of inertial waves from boundary turbulence in a librating sphere, *J. Fluid Mech.*, *728*, R5, doi:10.1017/jfm.2013.320.

Schaeffer, N., and P. Cardin (2005), Quasigeostrophic model of the instabilities of the Stewartson layer in flat and depth varying containers, *Phys. Fluids*, *17*, 104111, doi:10.1063/1.2073547.

Stewartson, K. (1966), On almost rigid rotations. Part 2, *J. Fluid Mech.*, *26*(1), 131–144.

Tilgner, A. (2007), Zonal wind driven by inertial modes, *Phys. Rev. Lett.*, *99*, 194501, doi:10.1103/PhysRevLett.99.194501.

Vanyo, J. P., P. Wilde, P. Cardin, and P. Olson (1995), Experiments on precessing flows in the Earth's liquid core, *Geophys. J. Int.*, *121*, 136–142.

Zhang, K., K. H. Chan, and X. Liao (2011), On fluid motion in librating ellipsoids with moderate equatorial eccentricity, *J. Fluid Mech.*, *673*, 468–479.

Zimmerman, D. S., S. A. Triana, H. C. Nataf, and D. P. Lathrop (2014), A turbulent, high magnetic Reynolds number experimental model of Earth's core, *J. Geophys. Res. Solid Earth*, *119*, 4538–4557, doi:10.1002/2013JB010733.